Jet-cooled ethylene cavity ring-down spectroscopy between 5880 and 6200 cm–1

Solène Perot, Julien Lecomte, Nicolas Suas-David, Lucile Rutkowski, Michael M. Rey, Samir Kassi, Andrei V. Nikitin, Robert Georges

Jet-cooled ethylene cavity ring-down spectroscopy between 5880 and 6200 cm^{-1}

Solène Perot[a], Julien Lecomte[a], Nicolas Suas-David[a], Lucile Rutkowski[a*], Michaël Rey[b], Samir Kassi[c], Andrei V. Nikitin[d], Robert Georges[a*]

[a]*IPR, UMR 6251, Université de Rennes, Rennes, France*
[b]*GSMA, UMR 7331, Université de Reims, Reims, France*
[c]*LIPhy, UMR 5588, Université Grenoble Alpes, Saint Martin d'Hères, France*
[d]*V.E. Zuev Institute of Atmospheric Optics, Russian Academy of Sciences, 1, Akademichesky Avenue, 634055 Tomsk, Russian Federation*

Key words: ethylene, near-infrared spectrum, variational calculations, jet-cooled CRDS

**Corresponding authors:* *robert.georges@univ-rennes.fr*
lucile.rutkowski@univ-rennes.fr

Abstract

Absorption spectra of jet-cooled ethylene (ethene, C_2H_4) are recorded at three different rotational temperatures (6/8 K, 12 K, 38 K) using cavity ring-down spectroscopy (CRDS) in the 5880-6200 cm^{-1} spectral region. Rotational cooling is used to determine the various vibrational band centers by simplifying drastically the rotational band structure. A line-by-line assignment, based on a direct comparison with the TheoReTS variational line list and a systematic use of lower state combination difference (LSCD), is performed. Experimental line lists including line position and line integrated absorption cross sections are drawn up. The 6/8 K, 12 K and 38 K spectra contain 668, 1553 and 1679 absorption lines respectively. Overall, 320 rovibrational lines are assigned across 20 interacting vibrational bands. Among the 20 vibrational cold bands identified in this work, 14 had never been observed before. Line intensities are in the range of 10^{-24} - 10^{-20} cm/molecule. A direct comparison between our work and the TheoReTS and ExoMol theoretical line lists, as well as with the recent experimental work of Ben Fathallah *et al.* 2024 is provided.

Highlights

- An innovative slit nozzle with adjustable opening is used to cool C2H4 down to 6 K
- Cavity ring-down spectroscopy provides high sensitivity in the 1.6-1.7 µm range
- Rotational cooling allows observation of 14 new vibrational bands
- 320 rovibrational lines are assigned to 20 bands using the TheoReTS linelist

1. Introduction

The high-temperature atmospheres (500 – 2000 K) of hot and warm Jupiter exoplanets [1] have revealed the presence of various organic molecules including carbon dioxide [2], water [2,3], hydrogen cyanide [4], carbon monoxide [4], ammonia [5], and recently sulfur dioxide [6]. As two small hydrocarbons (methane [2,7] and acetylene [5]) were also detected in these hot environments, the presence of other small hydrocarbons, such as ethylene (C_2H_4) is very likely, at least in exoplanets at moderate temperatures, i.e., below the dissociation temperature (~ 1000 K [8,9]) of the molecule. It is worth reminding that ethylene is also present in numerous gas giant atmospheres of our solar system including Jupiter [10], Saturn [11], Neptune [12], but also in the atmosphere of Titan [13]. Spatial telescopes and missions, such as the James Webb Space Telescope (JWST) [14] and the upcoming Ariel mission [15,16], aim at studying more extensively the hot Jupiter exoplanets. However, the quantitative analysis of the observations and the accurate modeling of the radiative properties of these atmospheres require first the extensive knowledge of the infrared absorption fingerprints of relevant molecules, such as ethylene, at temperatures found in hot Jupiters. Nevertheless, the spectroscopic data for ethylene is very scarce, partly due to its 12 vibrational modes leading to a highly congested spectrum, particularly in the near-infrared (near-IR), even at low temperatures. As a first analysis stage, before moving on to high-temperature spectroscopy, we performed a jet-cooled study to identify new cold band transitions of ethylene in the 1.6 - 1.7 µm spectral range (5880-6200 cm^{-1}) corresponding to the first overtone of CH stretching modes.

A series of ethylene spectroscopic studies were already published in the 1.6 - 1.7 µm spectral region. In 1988, 11 bands of a- and b-type were observed by Fourier transform infrared spectroscopy (FTS) at room temperature with a resolution of 0.5 cm^{-1} [17]. Ten years later, in 1998, the most intense $\nu_5 + \nu_9$ band was recorded by sub-doppler optothermal spectroscopy in the range 6080-6220 cm^{-1} with a resolution of 1.5×10^{-2} cm^{-1} (450 MHz), enabling the

unambiguous assignment of over 200 lines from which the spectroscopic constants of this band were derived [18]. Ethylene was also studied in the 5850-6200 cm^{-1} spectral range, using FTS [19] coupled with slit-jet expansion to lower its rotational temperature to 53 K. This study determined the band centers of six interacting vibrational bands, namely $\nu_2 + \nu_6 + \nu_9$, $\nu_2 + \nu_3 + \nu_{11}$, $\nu_1 + \nu_{11}$, $\nu_5 + \nu_{11}$, $\nu_1 + \nu_2 + \nu_{12}$ and $\nu_5 + \nu_9$. The latter band was studied using diode laser cavity ring-down spectroscopy (CRDS) in the 1.625 μm (6150 cm^{-1}) region. The position and intensity of 17 strong ^{Q}Q lines were recorded [20]. As the region around 6150 cm^{-1} exhibits a strong absorption, it was investigated for the detection of traces of ethylene using cavity enhanced photoacoustic spectroscopy [21]. An absorption spectrum of ethylene was recorded using a two-channel photo-acoustic spectrometer in the 6035-6210 cm^{-1} spectral range with a resolution of 3.34×10^{-4} cm^{-1} (10 MHz) at 293 K [22]. Another spectrum at 293 K was recorded between 6030 and 6250 cm^{-1} using FTS and a photo-acoustic spectrometer [23], from which an effective model was built by considering the two $\nu_5 + \nu_{11}$ and $\nu_5 + \nu_9$ bands as an interacting dyad, allowing to assign more than 600 transitions. More recently, a CRDS study on acetylene recorded 2500 unwanted ethylene lines due to an impurity in the sample [24]. To eliminate ethylene lines from their acetylene spectrum, the authors compiled an empirical list of over 12200 lines in the 5800-6400 cm^{-1} spectral range. This line list was then used to assign and confirm, by Lower State Combination Differences (LSCD), 1674 ethylene transitions to five bands [25] ($\nu_5+ \nu_9$, $\nu_5+ \nu_{11}$, $\nu_2+ \nu_3+ \nu_{11}$, $\nu_2+ \nu_6+ \nu_9$ and $\nu_1+ \nu_{11}$). Theoretical studies were also performed in this spectral region: a variational rovibrational line list in the 0-6400 cm^{-1} range was calculated at temperatures of 80, 160 and 296 K, and two line lists in the 0-5200 cm^{-1} range at 500 and 700 K [26], all are freely accessible on the TheoReTS database [27]. This work was subsequently extended up to 9000 cm^{-1} at 130 K and 296 K by Mraidi *et al.* [28]. A second theoretical rovibrational line list is also available in the ExoMol database from 0 to 7000 cm^{-1} at temperatures up to 700 K [29].

To date, a large number of interacting vibrational bands still remains to be isolated and assigned in the near-IR. Here, we aim to provide unambiguous line assignments of 14 new bands for the ethylene spectrum to extend the TheoReTS database in the 5880-6200 cm^{-1} spectral region. Our study is carried out at very low rotational temperatures under jet-cooled conditions in order to simplify the very dense rovibrational spectrum at room temperature, which in turn facilitates the assignment of rovibrational lines and thus the determination of the various interacting vibrational band centers. This paper is organized as follows. Section 2 describes the experimental setup and the various experimental conditions used in this work. Section 3 details the procedures used to extract the translational and rotational temperatures and density of C_2H_4 in supersonic flows. Section 4 describes the procedure used to assign the observed rovibrational transitions. Section 5 compares our data with the recent experimental work by Ben Fathallah et al.[3] and with the theoretical databases TheoReTS and ExoMol, before concluding in Section 6.

2. Experiment

The spectrometer used to probe the jet-cooled ethylene, presented in Figure 1, is similar to the one used in previous studies [30,31]. The sample (C_2H_4) and carrier gases (Ar or N_2) are injected into a high-pressure volume and then expanded through a slit nozzle into a vacuum chamber evacuated by 4 Edwards roots blowers (pXH 6000) connected in parallel and backed up by a 4000 m^3/h Alcatel pump in series with a 650 m^3/h Busch primary pump (CLFH 631), delivering a total pumping capacity of ~20,000 m^3/h. A Fabry-Perot cavity is mounted transversally to the supersonic jet and probed using a set of 13 fibered distributed feedback laser diodes (DFBs) (from NTT Electronics, Eblana photonics and FITEL) covering the 1.6 - 1.7 μm spectral range. Each diode is scanned from –10 °C to +60 °C using a custom proportional integral differential (PID) temperature stabilizer to cover ~7 nm (~30 cm^{-1}). The IR light beam is directed and

focused in the optical cavity with two steering planar mirrors and a converging lens (focal length 11 mm) used to inject the fundamental spatial mode of the cavity. While 10% of the optical power is directed to a wavemeter (HighFinesse WS7-60 series) to measure the laser frequency with a precision of 40 MHz, the remaining 90 % reaches an acousto-optic modulator (AOM FCM-40.8E5C IntraAction) used as an ultrafast optical switch, enabling the recording of ring-down events with a photodiode, on which the light beam is focused by a converging lens (focal length 40 mm). To match the cavity resonance with the instantaneous laser wavelength, the cavity output mirror is mounted onto a piezoelectric transducer (PZT) modulating the cavity length over a full free spectral range at a frequency of 50 Hz. Once acquired, an exponential decay curve is fitted to each ring-down event to obtain the ring-down time τ_{RD} (typically between 110 and 160 µs) and the absorption coefficient α is retrieved from equation (1), where τ_0 is the ring-down time of the empty cavity and c is the celerity of light in vacuum:

$$\alpha = \frac{1}{c\tau_{RD}} - \frac{1}{c\tau_0} \quad (1)$$

In practice, τ_0 is not measured but deduced from the variation of the broadband baseline on which the absorption lines lie. The high-finesse cavity (F > 200 000) consists of two high-reflectivity mirrors (> 99.99%, Layertec) mounted on bellows to limit vibrations caused by the pumping unit, and attached 84 cm apart at the end of two stainless steel tubes. The tubes are placed on both sides of the supersonic jet and flushed with dry nitrogen or argon to limit the absorption of warm residual C_2H_4 present in the expansion chamber. Gas mixtures of ethylene (Air Liquide, 99.95% purity) and argon (Air Liquide, 99.998% purity) or nitrogen (Air Liquide, 99.995% purity) are injected continuously using mass flow controllers (Bronkhorst). The mixtures are expanded through an 8.1 cm long slit nozzle with a tunable opening ranging from

10 to 320 µm into the low-pressure chamber, producing a planar supersonic expansion characterized by rotational temperatures ranging typically between 5 and 60 K.

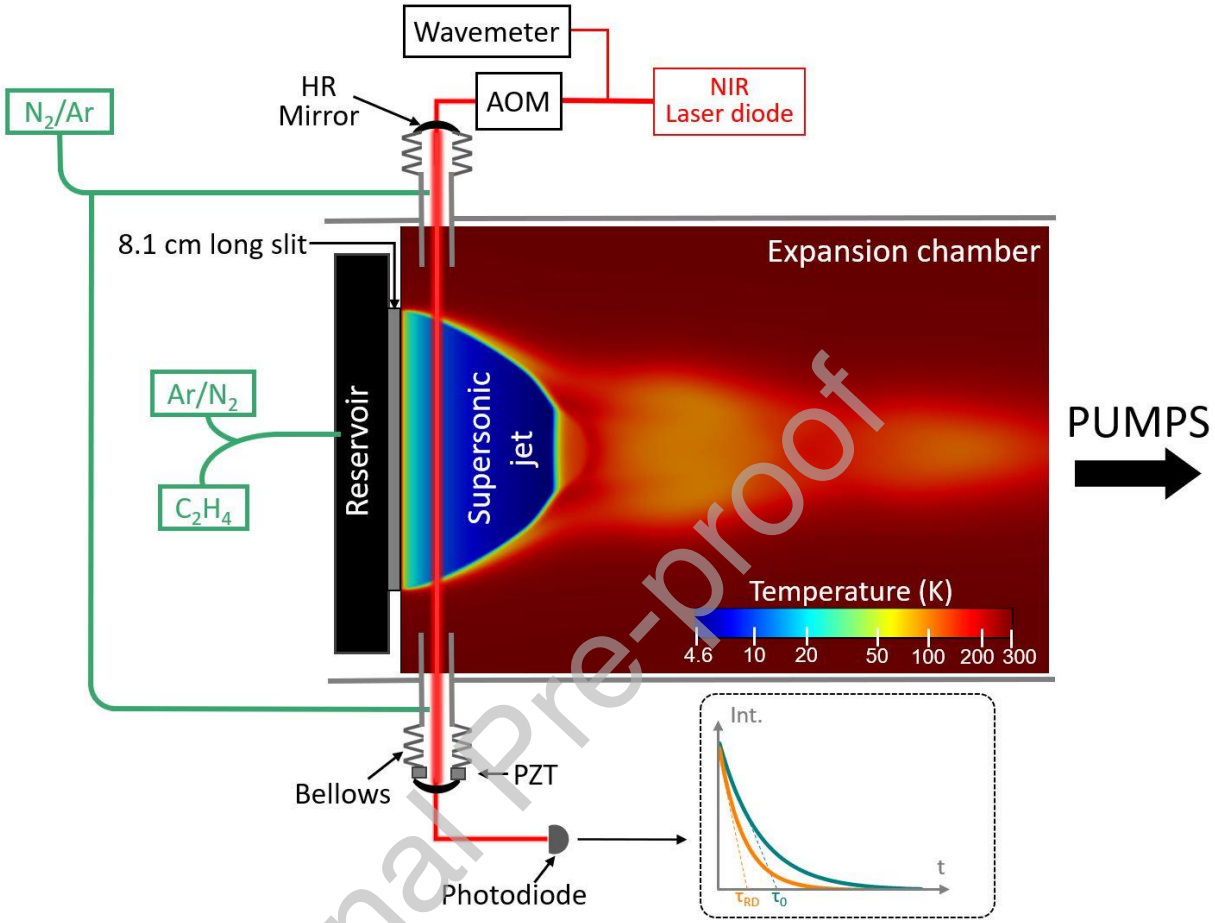

Fig. 1. Experimental setup used to record ethylene spectra (AOM: Acousto-optic modulator; PZT: piezoelectric transducer; HR Mirror: high-reflectivity mirror).

Ethylene spectra are recorded under three specific conditions giving rise to three different rotational temperatures (see Table 1). Condition 1 is chosen to obtain the coldest possible rotational temperature. The recording for this specific condition was carried out in two separate experimental campaigns, so that the low-wavenumber (< 5935 cm^{-1}) and high-wavenumber (> 6080 cm^{-1}) sides of the spectrum are in slightly different conditions, hereafter referred to as condition 1'. Conditions 2 and 3 are chosen to gradually increase the rotational temperature in order to observe absorption lines with higher *J*-values. To this end, the proportion of ethylene is increased, the slit width is increased to dampen cooling efficiency, the laser beam is

positioned closer to the slit aperture and argon is replaced by a diatomic gas (N_2) in condition 3 to temper the local Mach number of the flow.

Table 1: Experimental conditions used in this work

Experimental Condition no.	1	1'	2	3
C_2H_4 flow (sccm) [a] and relative concentration	12 (0.04 %)		30 (0.15 %)	60 (0.21 %)
Buffer gas flow (slm) [b]	Ar – 28		Ar – 20	N_2 – 28
Slit opening (µm)	30		270	320
Probing distance from nozzle (mm)	3		1	1
Chamber pressure (Torr)	0.17		0.13	0.15
Reservoir pressure (Torr)	80.3		52.7	56.0
T_{rot} (K)	6.3 ± 0.7	8.0 ± 0.5	12.0 ± 0.4	38.2 ± 1.5
T_{trans} (K)	5.5 ± 1.2	8.1 ± 1.0	14.8 ± 3	41.2 ± 5.9
Probed C_2H_4 number density (10^{12} molec.cm^{-3})	1.4 ± 0.2	1.7 ± 0.2	7.9 ±0.8	11.5 ± 1.2

[a] Standard cm^3/min (flow rate relative to a pressure of 1 atm and a temperature of 0 °C)
[b] Standard Liter/min (flow rate relative to a pressure of 1 atm and a temperature of 0 °C)

3. Spectra processing

3.1. Fitting procedure

Recorded spectra are shown in Figure 2. The effect of increasing the rotational temperature is particularly visible on the $\nu_5+\nu_9$ a-type band around 6150 cm^{-1}, which is the strongest absorption feature in the spectrum. As the temperature increases, the band extends to the sides, indicating the presence of absorption lines with higher *J*-values.

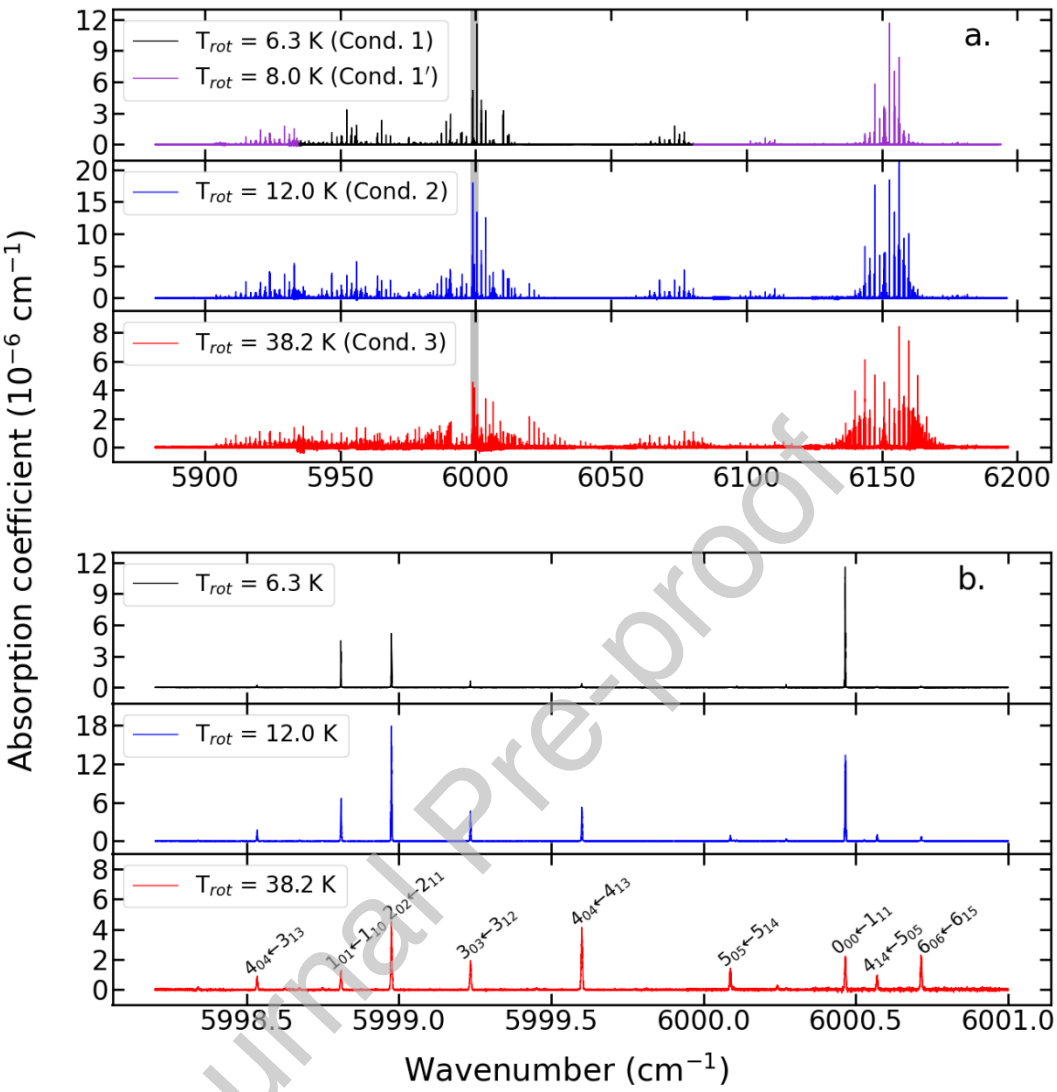

Fig. 2. (a) Overview of the ethylene spectra recorded at rotational temperatures of 6.3/8.0, 12.0 and 38.2 K. The shaded part of panel (a) is enlarged in panel (b). (b) Enlarged part of the spectrum illustrating the effects of temperature on line intensity and width in the band ν_5+ ν_{11}.

Spectral lines are automatically detected and fitted for the three experimental conditions studied using an in-house fitting procedure. The baseline is first determined by following the numerical algorithm “d” described in Ref. [32] and then fitted using a polynomial function. The absorption lineshapes are considered as purely thermally broadened, and collisional broadening as negligible because of the low molecular densities of C_2H_4 in the gas expansion (see Table

1). Therefore, gaussian profiles are fitted to each of the observed spectral lines. Experimental line lists including line position, line integrated absorption coefficient and line integrated absorption cross section are established for the three conditions and are provided as Supplementary Material. Examples of fitted transitions are displayed in Figure 3. Figure 3a depicts an isolated line fitted with a gaussian profile: the residuum shown in the lower panel is overall flat but exhibits an increased noise at the line wings, indicating a frequency noise estimated to be 10 MHz. The fitting procedure takes overlapping lines into account, as shown in Fig. 3b. In total, 1101 transitions are fitted for condition 1/1', 1941 for condition 2 and 2128 for condition 3.

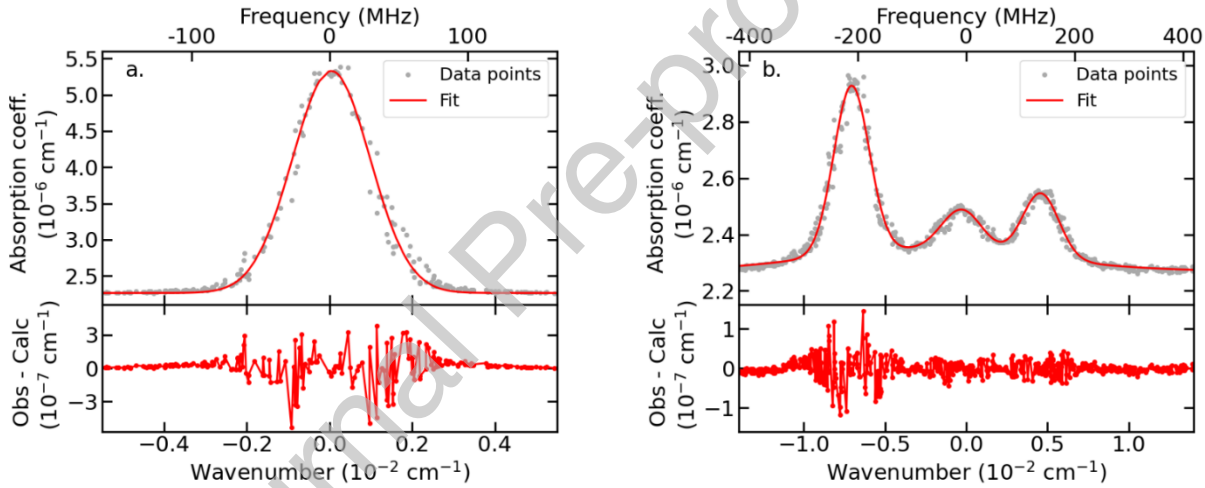

Figure 3. (a) Rovibrational absorption line, centered at 6151.13 cm^{-1}, fitted using a single gaussian line shape. (b) Three overlapping absorption lines, centered at 6150.83 cm^{-1}, fitted simultaneously using gaussian line shapes. Fit residuals are indicated in the lower panels.

The average standard deviation of the noise in our experiments is typically $\alpha_{min}^{cavity} = 5.6 \times 10^{-10}$ cm^{-1}. As the jet is probed over a distance of $l = 8{,}1$ cm, i.e., one tenth of the length of the cavity $L = 84$ cm, we consider that a transition can be detected if its amplitude is greater than $\alpha_{min}^{cavity} \times \frac{L}{l}$, leading to a minimum absorption coefficient of $\alpha_{min}^{jet} = 5.8 \times 10^{-9} cm^{-1}$. Given this sensitivity, Figure 4 illustrates the C_2H_4 density required to detect the R-branch rovibrational transitions of the most intense $\nu_5 + \nu_9$ band at different rotational temperatures using our

spectrometer. At very low temperature, the population of the lowest energy levels increases considerably, so that the required limiting density falls sharply for low *J*-value lines (a density of around 3×10^{10} molecules.cm^{-3} is needed to detect the R(0) line at 8 K), while it rises sharply for higher *J*-value lines. At 38 K (condition 3), the density required increases to around 10^{12}-10^{13} molec.cm^{-3} for the detection of lines with *J*-values up to 10.

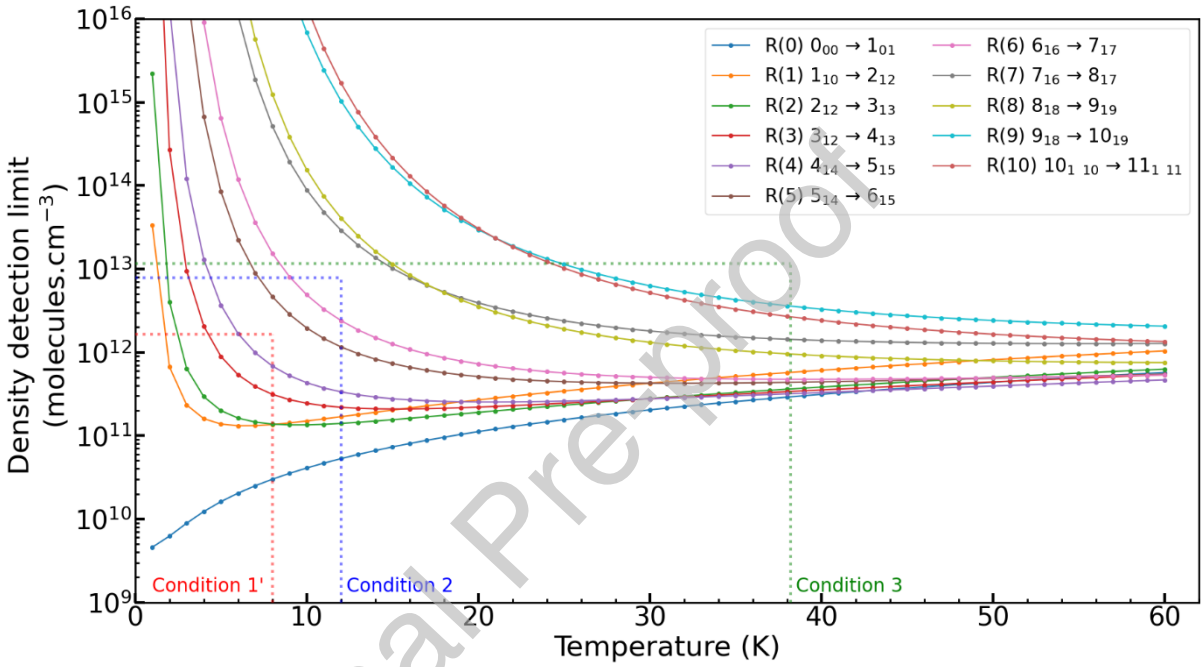

Fig. 4. Detectability limit of our experimental setup. C_2H_4 molecular density required to detect rovibrational lines in the R-branch of the $\nu_5 + \nu_9$ band at different rotational temperatures.

3.2. Translational temperature

The translational temperature, T_{trans}, is estimated from the linewidth of the transitions, assuming a Doppler broadening:

$$T_{Trans} = \left(\frac{c.FWHM}{\sqrt{8Rln(2)}\times\nu_0}\right)^2 \times M \qquad (2)$$

Here, $FWHM$ is the full-width at half maximum of each fitted transition (in cm^{-1}), c the celerity of light in vacuum, R the perfect gas constant, M the molar mass of the molecule and ν_0 the line position (in cm^{-1}) of the transition.

The translational temperatures extracted from the linewidths are relatively dispersed, as shown in Figure 5, which presents the set of translational temperatures extracted from the spectrum in condition 1. Ultimately, the central value of the dispersion curve was taken as the basis for defining the jet translational temperatures, listed in Table 1 for the different jet conditions used in this work. They range between 5.5 ± 1.2 K and 41.2 ± 5.9 K. The observed dispersion of the linewidths can have several origins. Firstly, the fit procedure is less accurate for weak transitions, resulting in greater uncertainty in the measured linewidth. Secondly, the infrared beam passes through the thin boundary layers (see Fig. 1), which are characterized by higher temperatures, and which contribute more to the absorption lines the higher the *J*-value. Finally, a more subtle effect, as already pointed out by Fleurbaey *et al*. [33], is linked to the continuous back-and-forth movement of the optical cavity mirror which is driven by the piezoelectric transducer and which is responsible for a Doppler line broadening. A frequency of 50 Hz is chosen in this study, leading to a compromise between reasonable acquisition time and limited line broadening.

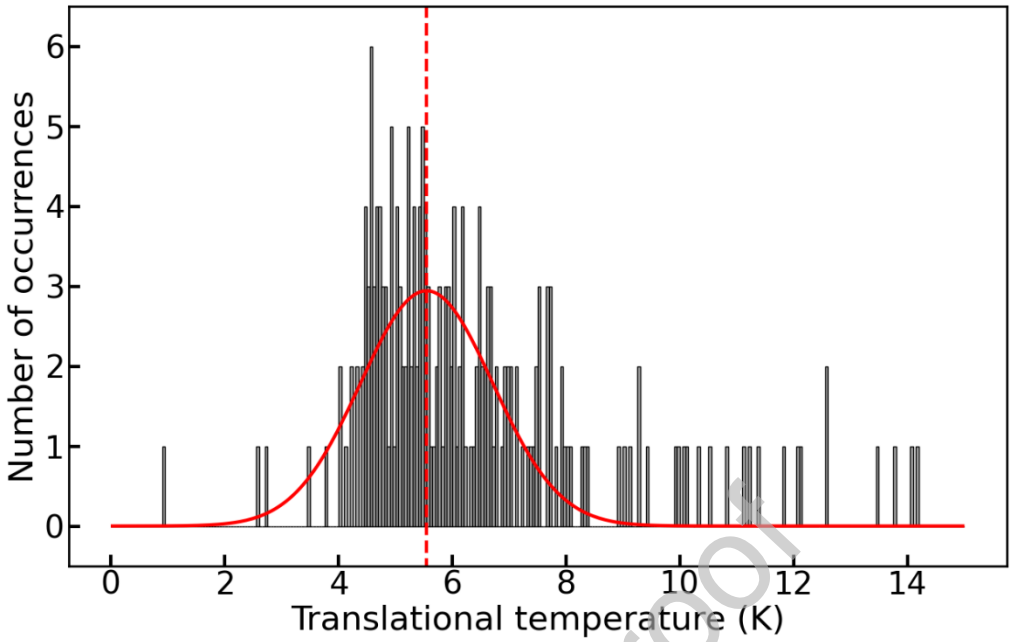

Fig. 5. Determination of the translational temperature from the linewidths for the ethylene spectrum recorded in condition 1. The distribution center is 5.5 ± 1.2 K.

3.3. Rotational temperature

A Boltzmann plot is used to determine the rotational temperature from the intensity of the lines recorded under each experimental condition (see Fig. 7). The following relationship is used:

$$log\left(\frac{\overline{\alpha}_{ij}\nu_{ij}^2}{A_{ij}g_j(2J+1)}\right) = \frac{-E_i}{k_B T_{rot}} \quad (3)$$

Where ν_{ij} is the wavenumber of the $j \leftarrow i$ transition, $\overline{\alpha}_{ij}$ is the line integrated absorption coefficient, A_{ij} is the Einstein A-coefficient, g_j is the statistical weight of the upper level j, E_i is the energy of the lower level i, T_{rot} is the rotational temperature, k_B is the Boltzmann's constant. The statistical weightg_j of the upper level, is expressed as the product of the electronic, vibrational and rotational statistical weights [34]:

$$g_j = g_e . g_v . g_r \quad (4)$$

Where g_e is the electronic statistical weight, g_v is the vibrational statistical weight, both of them are non-degenerate and are therefore taken to be 1. g_r is the rotational statistical weight calculated as follows:

$$g_r = (2J + 1).g_{sd}.g_{si} \quad (5)$$

Where J is the rotational quantum number of the considered state, g_{sd} is the state-dependent nuclear spin and g_{si} is the state-independent nuclear spin, which is equal to 1 for ethylene. Therefore, we calculate the statistical weight of a rovibronic level as:

$$g_j = (2J + 1).g_{sd} \quad (6)$$

The procedure for calculating g_{sd} is summarized in Table 2 for the special case of the vibrational state ν_5+ν_9 with B_{1u} symmetry. In Table 2, Γ_{Ψ_e}, Γ_{Ψ_v}, Γ_{Ψ_r} and $\Gamma_{\Psi_{SN}}$ are the irreducible representations of the electronic, vibrational, rotational and nuclear spin wavefunctions of the considered state, respectively, with $\Gamma_{\Psi_{evrSN}} = \Gamma_{\Psi_e} \times \Gamma_{\Psi_v} \times \Gamma_{\Psi_r} \times \Gamma_{\Psi_{SN}}$ the irreducible representation of the product of the latter wavefunctions. The Pauli principle imposes the symmetry of the total wavefunction, $\Gamma_{\Psi_{tot}}$ to be either A_g or A_u. Therefore, the g_{sd} of a particular rovibronic level is the coefficient corresponding to that symmetry in the $\Gamma_{\Psi_{evrSN}}$ product. If no functions of A_g or A_u symmetries are involved in the $\Gamma_{\Psi_{evrSN}}$ product, then the g_{sd} of that particular rovibronic level is 0. K_a and K_c are the quantum numbers associated with the projection of the rotational angular momentum on the *a* and *c* axis of the C_2H_4 asymmetric top molecule, respectively. As shown in Table 2, the nuclear spin statistical weight is 3 or 7, depending on the even (e) or odd (o) parity of the K_a and K_c quantum numbers.

Table 2. Determination of state-dependent nuclear spin statistical weights g_{sd} for the special case of a B_{1u} vibrational symmetry.

Γ_{ψ_e}	Γ_{ψ_v}	K_a K_c	Γ_{ψ_r}	$\Gamma_{\psi_{evr}}$	$\Gamma_{\psi_{SN}}$	$\Gamma_{\psi_{evrSN}}$	$\Gamma_{\psi_{tot}}$	g_{sd}
A_g	B_{1u}	e e	A_g	B_{1u}	$7A_g + 3B_{1g} + 3B_{2g} + 3B_{3g}$	$7B_{1u} + \mathbf{3A_u} + 3B_{3u} + 3B_{2u}$	$\mathbf{A_u}$	**3**
		e o	B_{1g}	A_u		$\mathbf{7A_u} + 3B_{1u} + 3B_{2u} + 3B_{3u}$	$\mathbf{A_u}$	**7**
		o e	B_{3g}	B_{2u}		$7B_{2u} + 3B_{3u} + \mathbf{3A_u} + 3B_{1u}$	$\mathbf{A_u}$	**3**
		o o	B_{2g}	B_{3u}		$7B_{3u} + 3B_{2u} + 3B_{1u} + \mathbf{3A_u}$	$\mathbf{A_u}$	**3**

For each experimental condition, a rotational temperature is extracted from the most intense vibrational bands using the Boltzmann plot method (Fig. 7). The rotational temperature given in Table 1 is the average value of these temperatures. For example, the temperature of 6.3 ± 0.7 K relative to condition 1 is determined from the bands $\nu_1 + \nu_2 + \nu_{12}$, $\nu_1 + \nu_{11}$ and $\nu_9 + 2\nu_{12}$, while the temperature of 8.0 ± 0.5 K relative to condition 1' is determined from the bands $\nu_2 + \nu_6 + \nu_9$, $\nu_1 + 2\nu_{10} + \nu_{12}$ and $\nu_5 + \nu_9$. In conditions 2 and 3, rotational temperatures are found to be ~ 3 K lower than translational ones. This unrealistic situation is linked to the uncertainty of temperature determination. Indeed, at such low sample concentrations (from 0.04 to 0.21%, see Table 1), the translational and rotational temperatures should be equivalent.

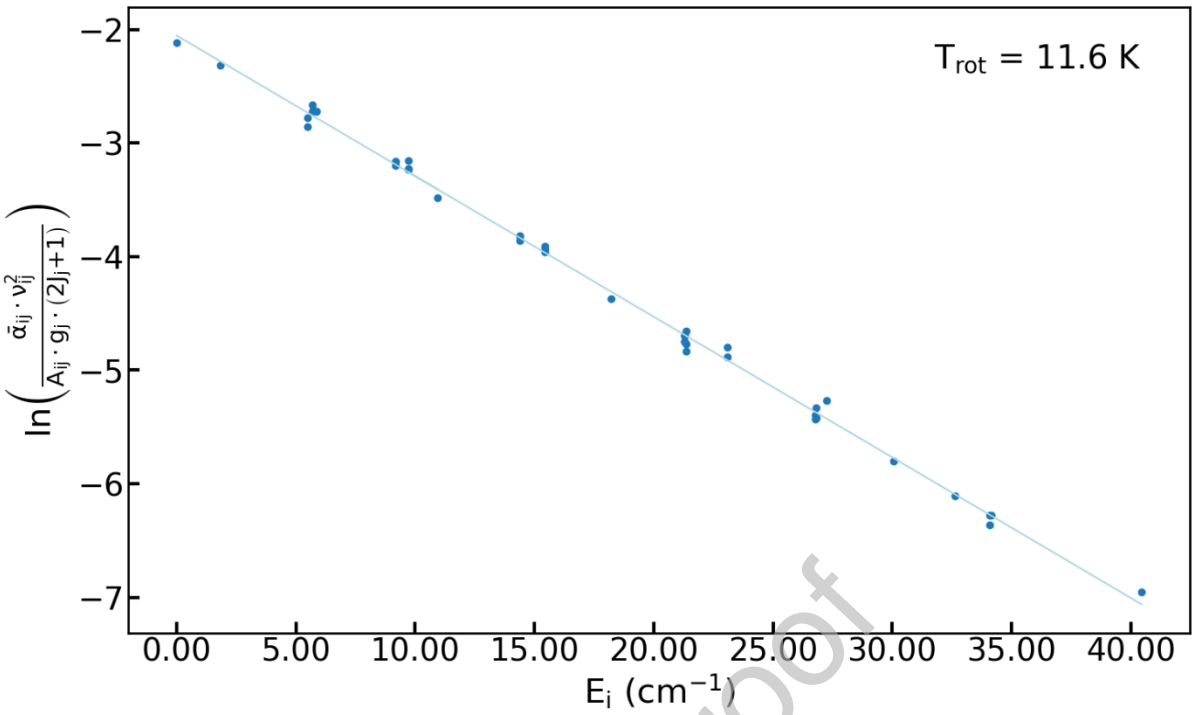

Fig. 6. Boltzmann plot for experimental condition 2 corresponding to the $\nu_5 + \nu_9$ band.

3.4. C_2H_4 number density

One of our objectives is to extract the line-integrated absorption cross section of the jet-cooled C_2H_4 (absolute intensity, $S_{C_2H_4}$) from the line-integrated absorption coefficient ($\overline{\alpha}_{C_2H_4}$) following the relationship:

$$S_{C_2H_4} = \frac{\overline{\alpha}_{C_2H_4}}{n_{C_2H_4}} \tag{8}$$

To do this, the local number density of C_2H_4 ($n_{C_2H_4}$) in the jet is first calibrated by matching the experimental absolute intensities to the calculated ones obtained from TheoReTS. This calibration is performed on the absorption lines of the $\nu_5 + \nu_9$ (condition 1'), $\nu_5 + \nu_{11}$ (condition 1), $\nu_5 + \nu_9$ and $\nu_5 + \nu_{11}$ bands (condition 2 and 3). As a result, number density of C_2H_4 varies from $1.4 \pm 0.2 \times 10^{12}$ molecules.cm^{-3} to $11.5 \pm 1.2 \times 10^{12}$ molecules.cm^{-3} (see Table 1).

4. Analysis and results

Line analysis is first carried out from the coldest and therefore simplest spectrum (condition 1/1'). As a preliminary approach, the experimental spectrum is compared with the spectrum simulated from the TheoReTS *ab initio* line list using SPVIEW software [35]. Observed low-*J* transitions matching to those simulated are quickly isolated and then confirmed using the lower state combination difference (LSCD). The assignment is considered confirmed if the difference between the centers of the two lines is equal to the expected LSCD ± 0.005 cm^{-1}, a tolerance corresponding to the uncertainty of the experimental setup. A P(1) transition, which cannot be confirmed by LSCD, is confirmed if its position within the band is consistent with the band type and its intensity is consistent with TheoReTS predictions. As a result, 140 rovibrational transitions are confirmed or newly assigned in 10 vibrational bands. A systematic LSCD check is then performed on the entire spectrum up to $J = 4$ transitions, leading to the assignment of 103 additional transitions in 11 additional vibrational bands. Overall, 243 transitions are confirmed or newly assigned in 20 vibrational bands, representing 36% of the lines detected for spectra recorded under condition 1/1'.

The spectra corresponding to conditions 2 and 3 are then processed. 49 additional transitions are confirmed by LSCD leading to a total of 290 assignments in 20 bands. To determine the band origins, each band is fitted using the Pgopher software [36] (see Fig.7).

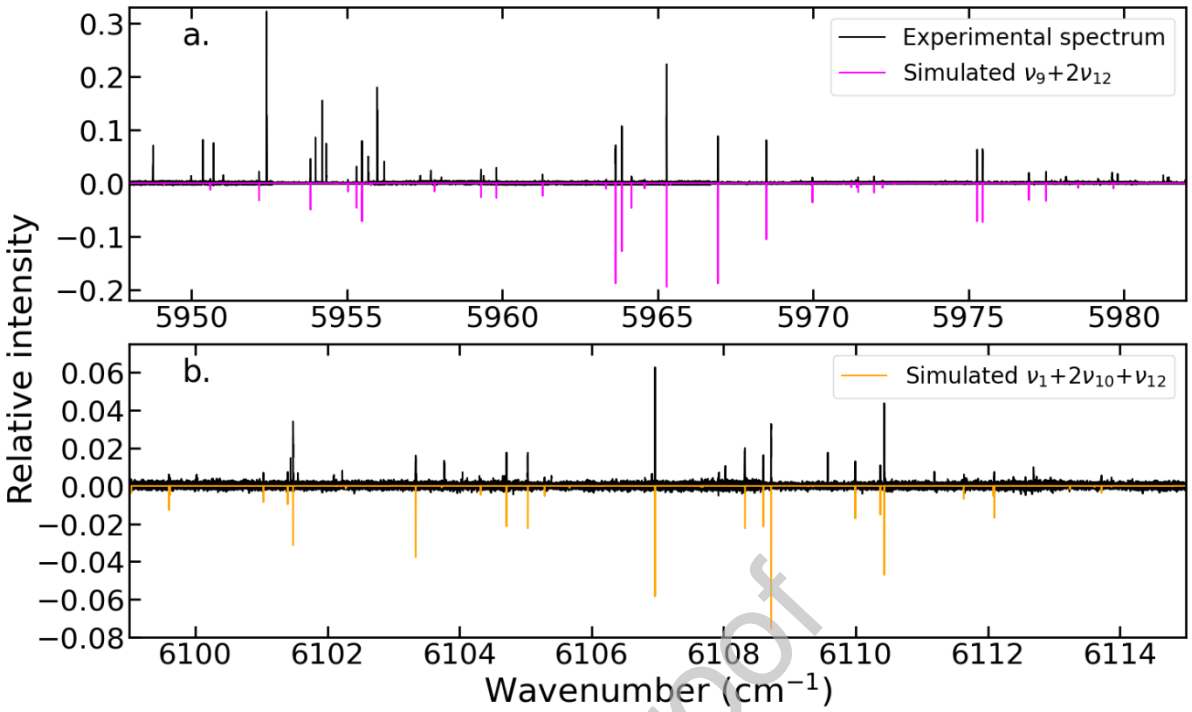

Fig. 7. Observed and simulated (Pgopher) spectra of $\nu_9+2\nu_{12}$ (panel a) and $\nu_1+2\nu_{10}+\nu_{12}$ (panel b) bands.

The fitted rotation-vibration molecular constants for each band are provided in supplementary materials. The fitting of the vibrational bands leads to additional line assignments. Finally, a total of 320 lines are assigned to 20 bands, representing 48 % of the spectrum (see Table 3 and Fig. 8). Due to the multiple interactions between the vibrational states located at 6000 cm^{-1}, it is not possible to assign an unambiguous vibrational label to each band. We therefore labeled the band according to the vibrational state that contributes most to the band (see the line list in the Supplementary Material).

Table 3. Vibrational band centers of C_2H_4 extracted from the experimental spectra.

Band label and symmetry	Band center (cm^{-1})	R0 (cm^{-1})	Number of attributions	Band intensity (calc.) (cm/molecule)	Band center determined by Georges *et al.*[37]
$2\nu_2+\nu_6+\nu_{12}$ (B_{3u})	5900.06717	5905.790	9	3.4714×10^{-21}	
$\nu_2+\nu_3+\nu_{11}$[a] (B_{1u})	5918.79341	5920.613	28	1.6855×10^{-20}	5927.57346
$\nu_2+\nu_6+\nu_9$[a] (B_{1u})	5927.59488	5929.411	20	9.2445×10^{-21}	5918.77176

$\nu_2+2\nu_6+\nu_7+\nu_8$ (B_{1u})	*Undetermined*[b]	5938.466	7	3.2899×10^{-21}	
$2\nu_{10}+3\nu_{12}$ (B_{1u})	*Undetermined*[b]	*undetermined*[c]	2	4.3555×10^{-21}	
$\nu_1+\nu_{11}$ (B_{1u})	5950.60178	5952.416	23	1.0291×10^{-20}	5950.58283
$\nu_9+2\nu_{12}$ (B_{3u})	5959.52497	5965.294	32	1.4653×10^{-20}	
$\nu_6+\nu_7+\nu_8+2\nu_{12}$ (B_{3u})	*Undetermined*[b]	5985.864	3	8.5571×10^{-22}	
$\nu_5+\nu_{11}$ (B_{3u})	5994.80663	6000.465	44	6.4046×10^{-20}	5994.7854
$\nu_3+2\nu_{10}+\nu_{11}$ (B_{1u})	*Undetermined*[b]	*undetermined*[c]	5	4.1390×10^{-21}	
$2\nu_2+\nu_3+\nu_{12}$ (B_{1u})	6031.77331	6033.580	6	3.9115×10^{-22}	
$\nu_1+\nu_2+\nu_{12}$ (B_{1u})	6071.59942	6073.415	26	1.3942×10^{-20}	6071.5755
$\nu_3+\nu_9+2\nu_{10}$ (B_{3u})	6104.02450	6109.578	6	1.1866×10^{-21}	
$\nu_1+2\nu_{10}+\nu_{12}$ (B_{1u})	6105.16700	6106.962	22	6.1714×10^{-21}	
$\nu_4+2\nu_7+\nu_8+\nu_{10}+\nu_{12}$[d] ($B_{1u}$)	6146.44391	6149.173	6	1.0793×10^{-20}	
$\nu_5+\nu_9$ (B_{1u})	6151.00199	6152.822	49	9.1913×10^{-20}	6150.98104
$\nu_5+2\nu_{10}+\nu_{12}$ (B_{3u})	*Undetermined*[b]	6156.151	9	3.5212×10^{-21}	
$\nu_4+\nu_6+\nu_7+\nu_{11}$ (B_{1u})	6159.43507	6161.266	8	4.1262×10^{-21}	
$\nu_2+\nu_5+\nu_{12}$ (B_{3u})	6171.85984	6177.496	8	1.1275×10^{-21}	
$\nu_5+\nu_6+\nu_7+\nu_8$ (B_{1u})	6176.16168	6177.977	7	1.6176×10^{-21}	

[a] The labels of these two bands are inverted in ref. [37]

[b] The band center cannot be determined because of a lack of observed transitions

[c] The R(0) line is not observed

[d] The identification of this 6-quanta band is highly speculative

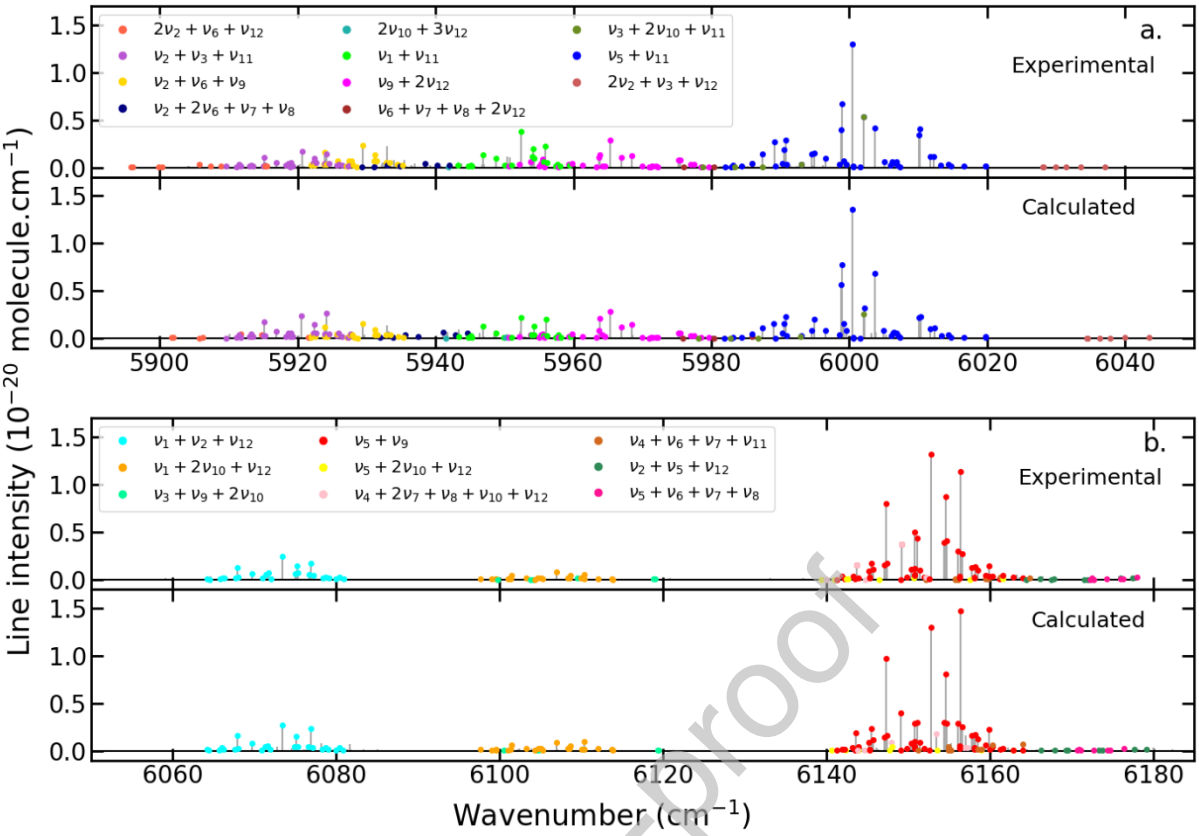

Fig. 8. Band by band overview of the assigned transitions. Upper panels: Experimental spectrum at 6/8 K (condition 1/1'). Lower panels: Simulated spectrum using TheoReTS. (a) From 5890 to 6050 cm^{-1}. (b) from 6050 to 6190 cm^{-1}.

5. Discussion

The assigned absorption lines are compared with the recent study by Ben Fathallah *et al.* [25] at room temperature (294 K) in the 5880-6200 cm^{-1} spectral range on 5 bands, namely $\nu_2+\nu_3+\nu_{11}$, $\nu_2+\nu_6+\nu_9$, $\nu_1+\nu_{11}$ and the two well-known strong bands $\nu_5+\nu_{11}$ and $\nu_5+\nu_9$. Our jet conditions limit the *J*-values to 5 for the strongest bands, so that only 114 observed lines can be compared with the results obtained by Ben Fathallah *et al.* [25] at LIPhy in Grenoble.

The measured absolute intensities (line-integrated absorption cross sections) are compared in figure 9. To carry out this comparison, the intensities of the 1/1' spectrum (6/8 K) obtained from Eq. (8) are converted to intensities at 294 K using the following relationship [38]:

$$S_{ij}(T_{rot}, T_{vib}) = S_{ij}(T_{ref}) \times \frac{Q(T_{ref})}{Q_{rot}(T_{rot})Q_{vib}(T_{vib})} \times exp\left[\frac{E_i}{k_B T_{ref}} - \frac{1}{k_B}\left(\frac{E_{v_i}}{T_{vib}} - \frac{E_{r_i}}{T_{rot}}\right)\right] \quad (11)$$

Where S_{ij} is the line intensity, Q, Q_{rot} and Q_{vib} are the total, rotational and vibrational partition functions, respectively, taken from the TheoReTS database. The lower vibrational energy level $E_{v_i} = 0$, since the observed transitions are exclusively cold band transitions. E_{r_i} is the lower rotational energy level. The vibrational temperature (T_{vib}) of the C_2H_4 molecule in the jet is assumed to be close to the nozzle throat temperature, i.e. ~ 220 K, which is too low to significantly populate the first excited vibrational energy level. The average intensity ratio between our measurements obtained under jet-cooled conditions and those obtained at room temperature by Ben Fathallah *et al.* [25] is 1.07 with a standard deviation of 1.41 (see Fig. 9), but with significant dispersion around this value. Indeed, with the exception of two lines in the $\nu_5+\nu_{11}$ band for which intensity ratios are > 7, intensity ratios are approximately between 0.5 and 2.

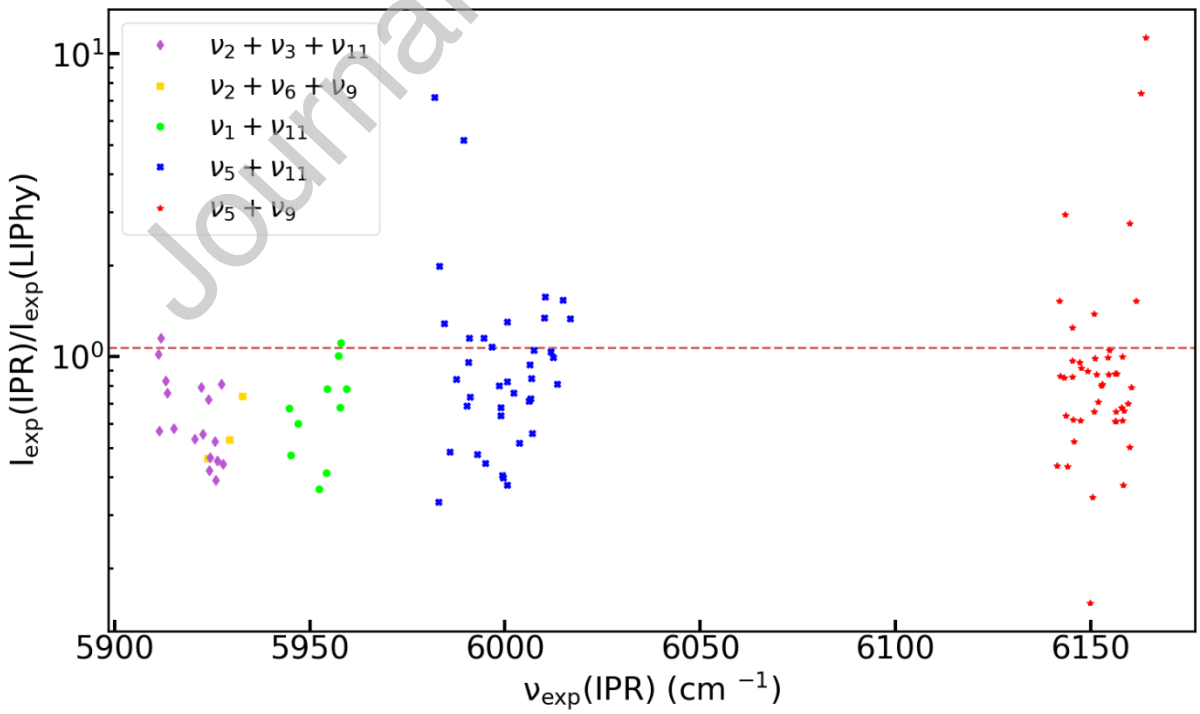

Fig. 9. Line intensity ratios between measurements obtained under jet-cooled conditions at IPR and room-temperature conditions by Ben Fathallah *et al.* [25] at LIPhy. Five bands,

distinguished by different colors and symbol shapes, have been considered. The horizontal dashed line represents the mean value (1.07).

Line positions of these 114 lines are also compared in Fig. 10 with those measured by Ben Fathallah *et al.* [25] Overall, the line positions are in good agreement, with the exception of a few lines which are probably differently assigned because the spectrum is crowded in this spectral region with many overlapping bands, particularly at room temperature.

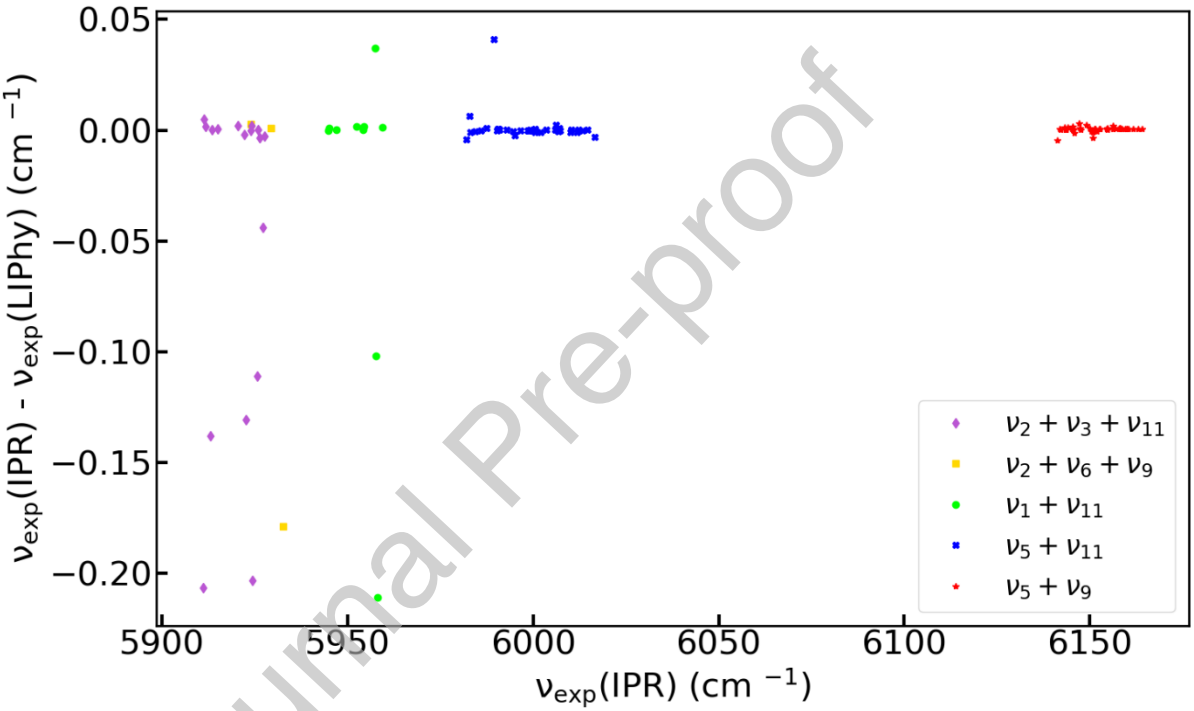

Fig. 10. Difference between experimental positions of lines with identical attributions. These positions were measured under jet-cooled conditions at IPR (this work) and at room temperature by Ben Fathallah *et al.* [25] at LIPhy. The five bands under consideration are distinguished by different colors and symbol shapes. The discrepancies observed are not due to measurement inaccuracy, but rather to a difference in line assignments.

The experimental line intensities are compared with the TheoReTS predicted intensities in Fig. 11. $I_{exp}/I_{TheoReTS}$ ratios between ½ and 2 are displayed in blue, those smaller than ½ or greater than 2 in red. The average ratio is 1.46 and the standard deviation of the values is 2.61. There are a number of reasons for this discrepancy. As already mentioned, some lines are very weak,

making their intensity determination uncertain. The experimental intensities we have measured should be regarded as estimates, not exact values.

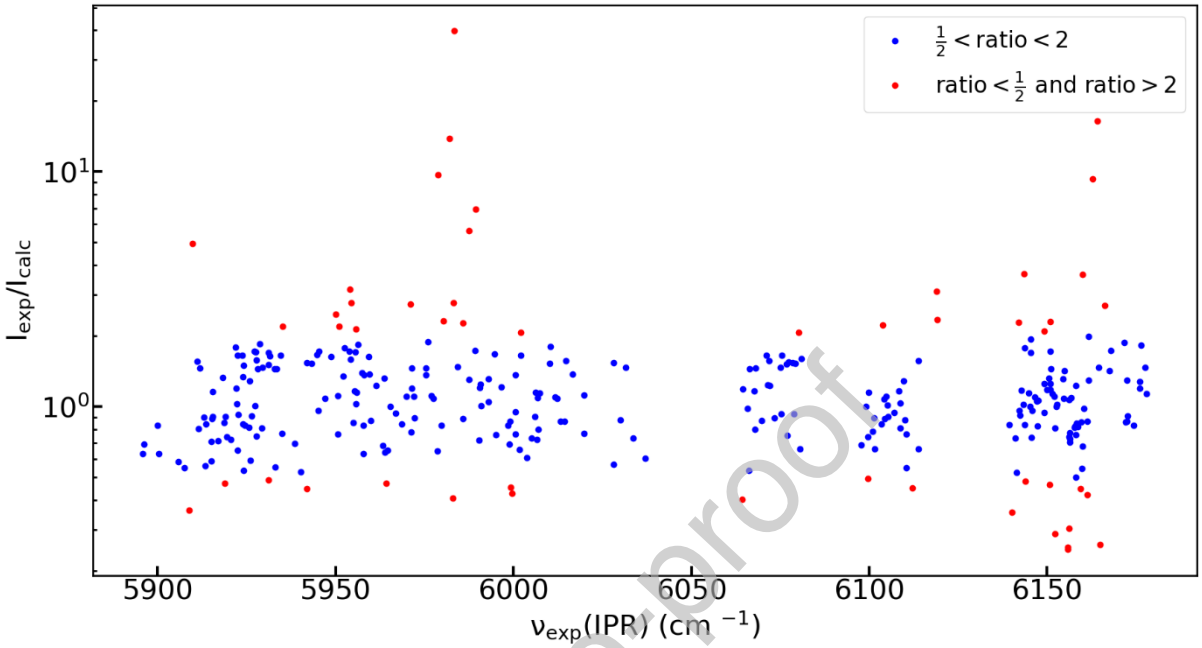

Fig. 11. Ratios of experimental intensity and intensity calculated by TheoReTS for the rovibrational lines identified. Ratios between ½ and 2 are shown in blue, those below ½ or above 2 in red.

The difference between experimental and calculated line positions is shown in Fig. 12. TheoReTS prediction for the $\nu_2+\nu_3+\nu_{11}$, $\nu_2+\nu_6+\nu_9$, $\nu_1+\nu_{11}$, $\nu_9+2\nu_{12}$, $\nu_5+\nu_{11}$, $\nu_1+\nu_2+\nu_{12}$, $\nu_1+2\nu_{10}+\nu_{12}$ and the $\nu_5+\nu_9$ bands is highly accurate ($|\nu_{exp} - \nu_{Calc}| \leq 0.1 cm^{-1}$). For some other bands, namely the $2\nu_2+\nu_6+\nu_{12}$, $\nu_2+2\nu_6+\nu_7+\nu_8$, $2\nu_2+\nu_3+\nu_{12}$, $\nu_3+\nu_9+2\nu_{10}$, $\nu_4+\nu_6+\nu_7+\nu_{11}$, $\nu_2+\nu_5+\nu_{12}$ and $\nu_5+\nu_6+\nu_7+\nu_8$ bands, the theoretical prediction for the band centers leads to a uniform and systematic shift of the entire band. The band origins determined in the present study will be used to easily correct the systematic deviations of the TheoReTS model. In other cases, as for bands $\nu_5+2\nu_{10}+\nu_{12}$, $\nu_4+2\nu_7+\nu_8+\nu_{10}+\nu_{12}$, and $\nu_3+2\nu_{10}+\nu_{11}$, the line positions are unevenly offset throughout the band, indicating a more complex network of interactions.

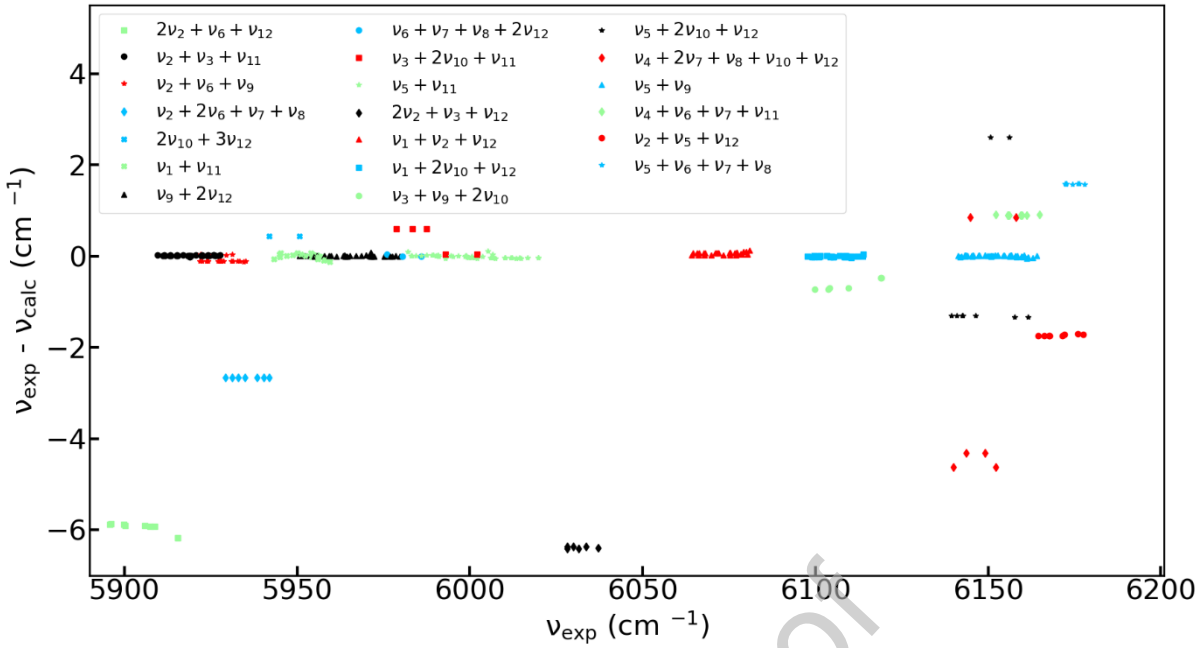

Fig. 12. Difference between experimental and TheoReTS line positions.

Finally, our spectra are compared with the ethylene line list[24] provided by the Exomol database. A state-to-state comparison is not possible between these two line lists, as molecular vibrations are described in terms of local modes in the ExoMol database and in terms of and normal modes in the TheoReTS database, used in the present work. Figs. 13, 14 and 15 show a bird-eye comparison between the experimental spectrum at 6/8 K and the TheoReTS and ExoMol predictions. The overall comparison is good (see Fig. 13), but some discrepancies are revealed by enlarged views (see Figs. 14 and 15).

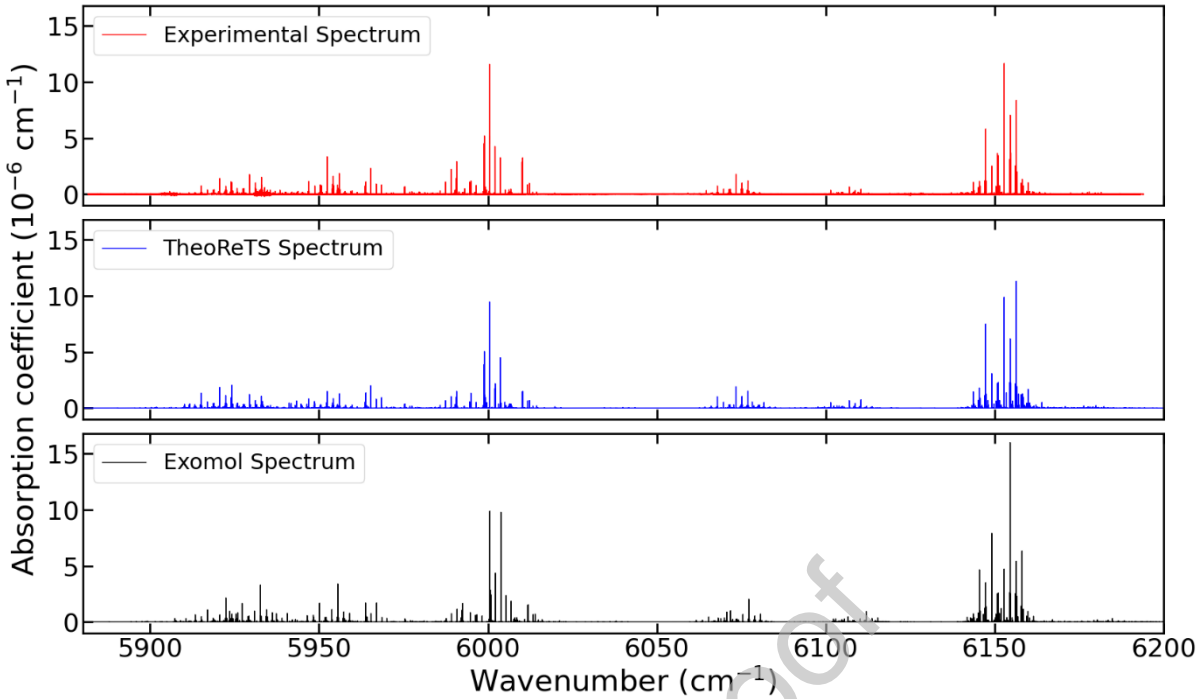

Fig. 13. Upper panel: Experimental spectrum at 6/8 K (condition 1/1'). Middle panel: TheoReTS spectrum. Lower panel: ExoMol spectrum.

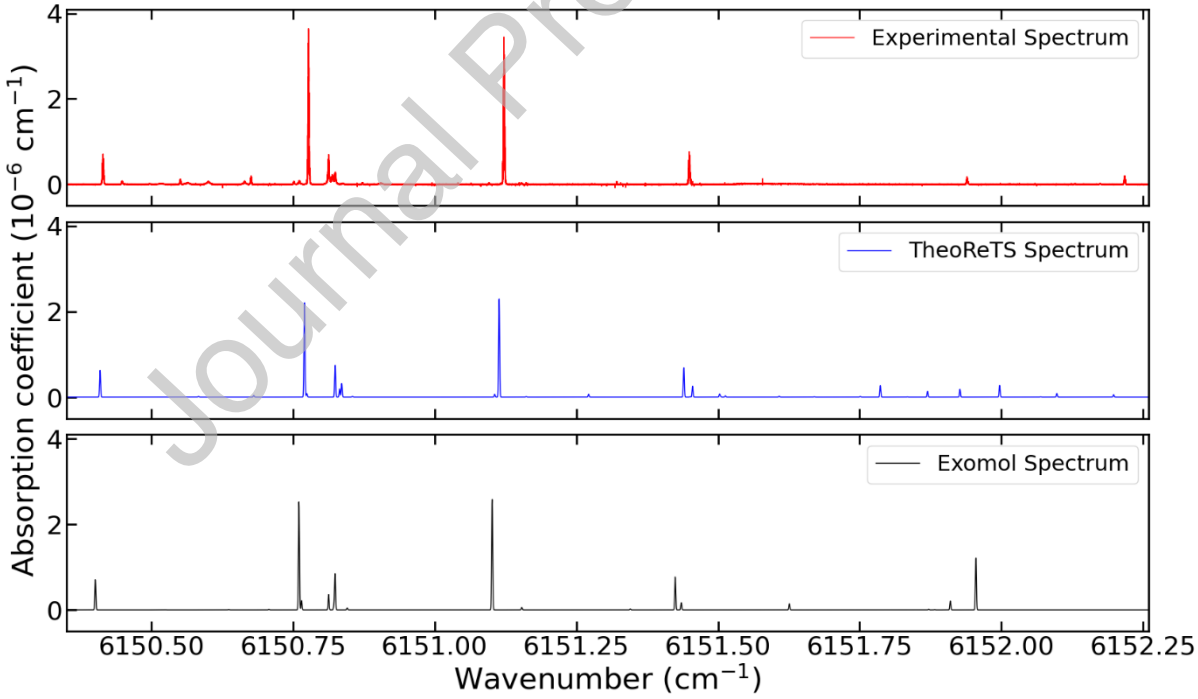

Fig. 14. Upper panel: Experimental spectrum at 6/8 K (condition 1/1'). Middle panel: TheoReTS spectrum. Lower panel: ExoMol spectrum.

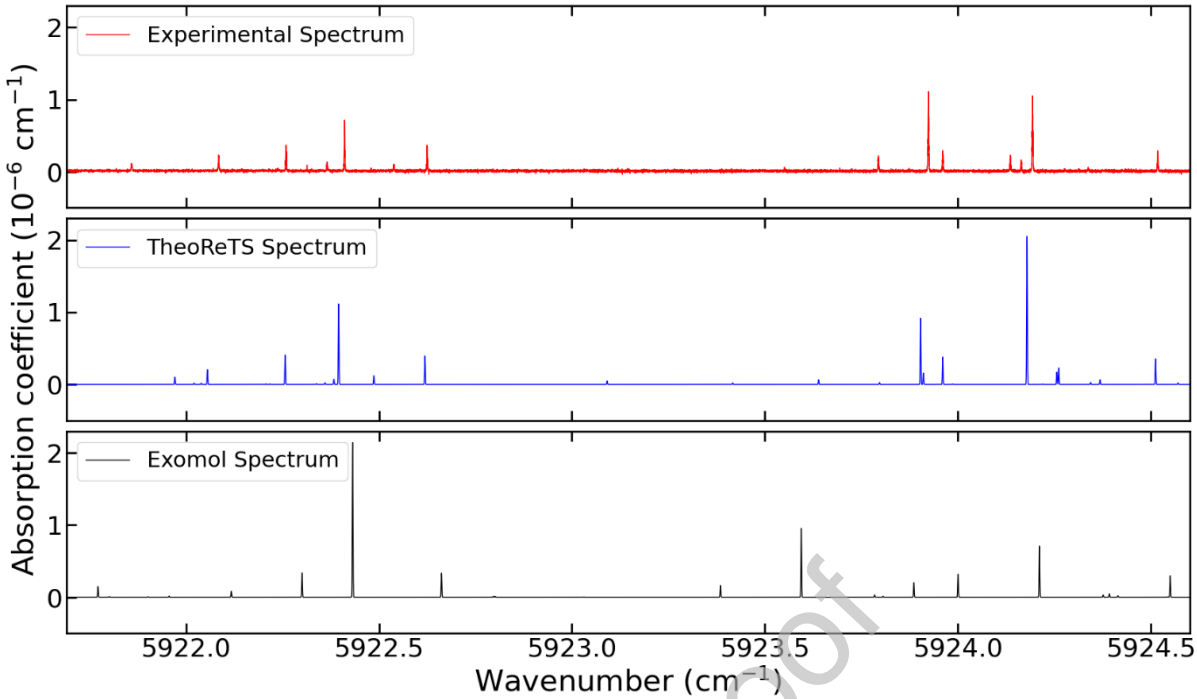

Fig. 15. Upper panel: Experimental spectrum at 6/8 K (condition 1/1'). Middle panel: TheoReTS spectrum. Lower panel: ExoMol spectrum.

6. Conclusion

This paper provides rovibrational assignments for the ethylene spectrum in the 5880-6200 cm^{-1} spectral range recorded under jet-cooled conditions at rotational temperatures of 6/8 K, 12 K and 38 K. In this spectral range, the high density of vibrational states and the multiple interactions between these different states lead to a particularly dense and complex spectrum at room temperature. The spectral simplification achieved by drastically lowering the rotational temperature has made it possible to isolate 20 vibrational bands and to assign 290 rovibrational lines in the 6/8 K spectrum. Among these 20 bands, 14 had never been reported in the literature before. These newly observed bands are tentatively assigned on the basis of the TheoReTS database. The newly determined band centers will be used to constrain variational calculations and improve the accuracy of TheoReTS. Our spectra at 12 and 38 K are currently being analyzed to assign higher *J*-value transitions. New ethylene spectra will soon be recorded in

hypersonic flow under non-LTE conditions ($T_{vib} \gg T_{rot}$) to identify the multiple hot bands expected to dominate the infrared spectrum at temperatures relevant to hot Jupiters.

Acknowledgements

We acknowledge funding from the Agence Nationale de la Recherche (CECoSA ANR-19-CE30-0038, ePYTHEAS ANR-16-CE31-0005 and ANR-RNF TEMMEX-ANR-21-3 0 CE-0053-01). MR acknowledges support from the Romeo computer center of Reims Champagne-Ardenne. We would like to thank Dr. Ons Ben Fathallah and Dr. Alain Campargue for our fruitful discussions, and Vincent Boudon and Cyril Richard for their help with the SPVIEW software.

References

[1] Tinetti G, Encrenaz T, Coustenis A. Spectroscopy of planetary atmospheres in our Galaxy. Astron Astrophys Rev 2013;21:63. https://doi.org/10.1007/s00159-013-0063-6.
[2] Swain MR, Tinetti G, Vasisht G, Deroo P, Griffith C, Bouwman J, et al. WATER, METHANE, AND CARBON DIOXIDE PRESENT IN THE DAYSIDE SPECTRUM OF THE EXOPLANET HD 209458b. ApJ 2009;704:1616. https://doi.org/10.1088/0004-637X/704/2/1616.
[3] Sing DK, Fortney JJ, Nikolov N, Wakeford HR, Kataria T, Evans TM, et al. A continuum from clear to cloudy hot-Jupiter exoplanets without primordial water depletion. Nature 2016;529:59–62. https://doi.org/10.1038/nature16068.
[4] Snellen IAG, de Kok RJ, de Mooij EJW, Albrecht S. The orbital motion, absolute mass and high-altitude winds of exoplanet HD 209458b. Nature 2010;465:1049–51. https://doi.org/10.1038/nature09111.
[5] Giacobbe P, Brogi M, Gandhi S, Cubillos PE, Bonomo AS, Sozzetti A, et al. Five carbon- and nitrogen-bearing species in a hot giant planet's atmosphere. Nature 2021;592:205–8. https://doi.org/10.1038/s41586-021-03381-x.
[6] Taylor J, Kirk J, Bell T, Barstow J, Gao P, Bean J, et al. Sulfur dioxide in the mid-infrared transmission spectrum of WASP-39b. Nature 2024;626. https://doi.org/10.1038/s41586-024-07040-9.
[7] Swain MR, Vasisht G, Tinetti G. The presence of methane in the atmosphere of an extrasolar planet. Nature 2008;452:329–31. https://doi.org/10.1038/nature06823.
[8] Silcocks CG, Travers MW. The kinetics of the thermal decomposition and polymerization of ethane and ethylene. Proceedings of the Royal Society of London Series A Mathematical and Physical Sciences 1997;233:465–79. https://doi.org/10.1098/rspa.1956.0004.
[9] Boyd ML, Wu T-M, Back MH. Kinetics of the thermal reactions of ethylene. Part I. Can J Chem 1968;46:2415–26. https://doi.org/10.1139/v68-394.
[10] Kostiuk T, Romani P, Espenak F, Livengood TA, Goldstein JJ. Temperature and abundances in the Jovian auroral stratosphere: 2. Ethylene as a probe of the microbar region. Journal of Geophysical Research: Planets 1993;98:18823–30. https://doi.org/10.1029/93JE01332.
[11] Bézard B, Moses JI, Lacy J, Greathouse T, Richter M, Griffith C. Detection of Ethylene (C2H4) on Jupiter and Saturn in Non--Auroral Regions 2001;33:22.07.

[12] Schulz B, Encrenaz T, Bezard B, Romani PN, Lellouch E, Atreya SK. Detection of C2H4 Neptune from ISO/PHT-S Observations. Journal of Astrophysical and Astrophysics Letters 1999.
[13] Roe HG, de Pater I, McKay CP. Seasonal variation of Titan's stratospheric ethylene (C2H4) observed. Icarus 2004;169:440–61. https://doi.org/10.1016/j.icarus.2004.01.002.
[14] Webb Image Release- Webb Space Telescope GSFC/NASA n.d. https://webb.nasa.gov/ (accessed April 15, 2024).
[15] Ariel Space Mission – European Space Agency M4 Mission n.d. https://arielmission.space/ (accessed April 15, 2024).
[16] Chubb KL, Robert S, Sousa-Silva C, Yurchenko SN, Allard NF, Boudon V, et al. Data availability and requirements relevant for the Ariel space mission and other exoplanet atmosphere applications 2024. https://doi.org/10.48550/arXiv.2404.02188.
[17] Duncan JL, Ferguson AM. Local mode and normal mode interpretations of the CH and CD stretching vibrational manifolds in C2H4 and C2D4. The Journal of Chemical Physics 1988;89:4216–26. https://doi.org/10.1063/1.454806.
[18] Platz T, Demtröder W. Sub-Doppler optothermal overtone spectroscopy of ethylene and dichloroethylene. Chemical Physics Letters 1998;294:397–405. https://doi.org/10.1016/S0009-2614(98)00885-9.
[19] BACH M, GEORGES R, HERMAN M, PERRIN A. Investigation of the fine structure in overtone absorption bands of 12C2H4. Molecular Physics 1999;97:265–77. https://doi.org/10.1080/00268979909482828.
[20] Parkes AM, Lindley RE, Orr-Ewing AJ. Absorption cross-sections and pressure broadening of rotational lines in the ν5 + ν9 band of ethene measured by diode laser cavity ring down spectroscopy. Phys Chem Chem Phys 2004;6:5313–7. https://doi.org/10.1039/B413238F.
[21] Rossi A, Buffa R, Scotoni M, Bassi D, Iannotta S, Boschetti A. Optical enhancement of diode laser-photoacoustic trace gas detection by means of external Fabry-Perot cavity. Applied Physics Letters 2005;87:041110. https://doi.org/10.1063/1.2000341.
[22] Kapitanov VA, Ponomarev YuN. High resolution ethylene absorption spectrum between 6035 and 6210 cm-1. Appl Phys B 2008;90:235–41. https://doi.org/10.1007/s00340-007-2920-3.
[23] Loroño Gonzalez MA, Boudon V, Loëte M, Rotger M, Bourgeois M-T, Didriche K, et al. High-resolution spectroscopy and preliminary global analysis of C–H stretching vibrations of C2H4 in the 3000 and 6000 cm−1 regions. Journal of Quantitative Spectroscopy and Radiative Transfer 2010;111:2265–78. https://doi.org/10.1016/j.jqsrt.2010.04.010.
[24] Lyulin OM, Mondelain D, Béguier S, Kassi S, Auwera JV, Campargue A. High-sensitivity CRDS absorption spectroscopy of acetylene between 5851 and 6341 cm−1. Molecular Physics 2014.
[25] Ben Fathallah O, Rey M, Campargue A. Analysis of the high resolution absorption spectrum of ethylene between 5800 and 6400 cm−1. Journal of Quantitative Spectroscopy and Radiative Transfer 2024;316:108905. https://doi.org/10.1016/j.jqsrt.2024.108905.
[26] Rey M, Delahaye T, Nikitin AV, Tyuterev VG. First theoretical global line lists of ethylene (12C2H4) spectra for the temperature range 50−700 K in the far-infrared for quantification of absorption and emission in planetary atmospheres. A&A 2016;594:A47. https://doi.org/10.1051/0004-6361/201629004.
[27] Rey M, Nikitin AV, Babikov YL, Tyuterev VG. TheoReTS – An information system for theoretical spectra based on variational predictions from molecular potential energy and dipole moment surfaces. Journal of Molecular Spectroscopy 2016;327:138–58. https://doi.org/10.1016/j.jms.2016.04.006.

[28] Mraidi S, Manceron L, Rey M, Aroui H, Campargue A. High resolution spectroscopy and a theoretical line list of ethylene between 5000 and 9000 cm−1. Journal of Quantitative Spectroscopy and Radiative Transfer 2023;310:108734. https://doi.org/10.1016/j.jqsrt.2023.108734.
[29] Mant BP, Yachmenev A, Tennyson J, Yurchenko SN. ExoMol molecular line lists – XXVII. Spectra of C2H4. Monthly Notices of the Royal Astronomical Society 2018;478:3220–32. https://doi.org/10.1093/mnras/sty1239.
[30] Louviot M, Suas-David N, Boudon V, Georges R, Rey M, Kassi S. Strong thermal nonequilibrium in hypersonic CO and CH4 probed by CRDS. The Journal of Chemical Physics 2015;142:214305. https://doi.org/10.1063/1.4921893.
[31] Dudás E, Suas-David N, Brahmachary S, Kulkarni V, Benidar A, Kassi S, et al. High-temperature hypersonic Laval nozzle for non-LTE cavity ringdown spectroscopy. The Journal of Chemical Physics 2020;152:134201. https://doi.org/10.1063/5.0003886.
[32] Morháč M. An algorithm for determination of peak regions and baseline elimination in spectroscopic data. Nuclear Instruments and Methods in Physics Research Section A: Accelerators, Spectrometers, Detectors and Associated Equipment 2009;600:478–87. https://doi.org/10.1016/j.nima.2008.11.132.
[33] Fleurbaey H, Čermák P, Campargue A, Kassi S, Romanini D, Votava O, et al. 12CO2 transition frequencies with kHz-accuracy by saturation spectroscopy in the 1.99–2.09 μm region. Phys Chem Chem Phys 2023;25:16319–30. https://doi.org/10.1039/D3CP01603J.
[34] Šimečková M, Jacquemart D, Rothman LS, Gamache RR, Goldman A. Einstein *A*-coefficients and statistical weights for molecular absorption transitions in the *HITRAN* database. Journal of Quantitative Spectroscopy and Radiative Transfer 2006;98:130–55. https://doi.org/10.1016/j.jqsrt.2005.07.003.
[35] Wenger Ch, Boudon V, Rotger M, Sanzharov M, Champion J-P. XTDS and SPVIEW: Graphical tools for the analysis and simulation of high-resolution molecular spectra. Journal of Molecular Spectroscopy 2008;251:102–13. https://doi.org/10.1016/j.jms.2008.01.011.
[36] Western CM. PGOPHER: A program for simulating rotational, vibrational and electronic spectra. Journal of Quantitative Spectroscopy and Radiative Transfer 2017;186:221–42. https://doi.org/10.1016/j.jqsrt.2016.04.010.
[37] GEORGES R, BACH M, HERMAN M. The vibrational energy pattern in ethylene (12C2H4). Molecular Physics 1999;97:279–92. https://doi.org/10.1080/00268979909482829.
[38] Dudás E, Vispoel B, Gamache RR, Rey M, Tyuterev VG, Nikitin AV, et al. Non-LTE spectroscopy of the tetradecad region of methane recorded in a hypersonic flow. Icarus 2023;394:115421. https://doi.org/10.1016/j.icarus.2022.115421.

Credit author statement

Solène Perot: Investigation, Formal analysis, Software, Writing Original Draft, Visualization. **Julien Lecomte**: Methodology. **Nicolas Suas-David**: Methodology, Investigation. **Lucile Rutkowski***:* Funding acquisition, Supervision, Writing – Review & Editing. **Michaël Rey**: Methodology, Software, Funding acquisition: **Samir Kassi**: Methodology. **Andrei V. Nikitin**: Methodology, Funding acquisition. **Robert Georges**: Conceptualization, Methodology, Supervision, Writing – Review & Editing, Project administration.

Declaration of interests

☒ The authors declare that they have no known competing financial interests or personal relationships that could have appeared to influence the work reported in this paper.

☐ The authors declare the following financial interests/personal relationships which may be considered as potential competing interests.